Ultrasonics - Sonochemistry 61 (2020) 104807

Contents lists available at ScienceDirect

Ultrasonics - Sonochemistry

journal homepage: www.elsevier.com/locate/ultson

Improvement of oxidation resistance of polymer-based nanocomposites through sonication of carbonaceous nanoparticles

Rosalia Teresi[a], Salvatore Marullo[b], Cristian Gambarotti[c], Filippo Parisi[d], Bartolomeo Megna[a], Giuseppe Lazzara[d], Francesca D'Anna[b], Nadka Tzankova Dintcheva[a,*]

[a] Università degli Studi di Palermo, Dipartimento di Ingegneria, Viale delle Scienze, Ed. 6, 90128 Palermo, Italy
[b] Università degli Studi di Palermo, Dipartimento STEBICEF, Viale delle Scienze, Ed. 17, 90128 Palermo, Italy
[c] Politecnico di Milano, Dipartimento di Chimica, Materiali ed Ingegneria Chimica "G. Natta", Piazza L. da Vinci 32, 20133 Milano, Italy
[d] Università degli Studi di Palermo, Dipartimento di Fisica e Chimica, Viale delle Scienze, Ed. 17, 90128 Palermo, Italy

ARTICLE INFO

Keywords:
Radical scavenging activity
CNTs
CB
UHMWPE
Oxidation resistance

ABSTRACT

The work aim is focused on two different aspects: *first*, the investigation of the effect of extended ultra-sound-assisted treatment (us) of carbonaceous nanoparticles, such as carbon nanotubes (CNTs) and carbon black (CB), on their radical scavenging activity, and *second*, the investigation of the oxidative resistance of polymer-based nanocomposites, containing us-treated CNTs and CB. Particularly, the CNTs and CB have been subjected to us sonication for different time intervals and the performed analysis reveals that both kinds of nanoparticles show decreased average hydrodynamic diameters and large content of surface defects. Really, the increased content of CNTs and CB defects, achieved during the sonication time, leads to an increased reactivity toward 1,1-diphenyl-2-pycryl (DPPH) radicals and an enhanced anti-oxidant activity toward macro-radicals, coming from the photo-degradation of the host polymer matrix. The studies of photo-oxidative behavior of the nanocomposites, based on Ultra High Molecular Weight (UHMWPE), reveal that the us treatment of the nanoparticles has a benefic effect on the oxidative resistance of the nanocomposites, especially at long exposure times. Overall, the ultra-sound-assisted treatment can be considered twofold powerful tool: (i) for disruption of the nanoparticles aggregations, and (ii) for capitalization of surface defects, amplifying and tuning in a controlled way the radical scavenging activity of the carbonaceous nanoparticles.

1. Introduction

Carbonaceous nanoparticles, as graphene (G), carbon nanotubes (CNTs) and carbon black (CB), have gained great interest due to their reinforcement action and peculiar properties, such as electric and thermal conductivity [1], mechanical and thermo-mechanical resistance [2], radical scavenging activity [3], etc. Therefore, in the last two decades, the ability of some carbonaceous nanoparticles to act as efficient free-radical traps has been successfully predicted by the Density Functional Theory (DFT), and as documented recently, the reactions between CNTs and free radicals can be explained theoretically through two different mechanisms, specifically, the electron-transfer and adduct formation, also considering the influence of the CNTs length, diameter, chirality and possible surface functionalization [4,5].

The CNTs radical scavenging activities can be understood considering their unique acceptor-like electronic properties, arising from the peculiar electronic structure. In fact, the CNTs electron donor and acceptor capability, which indicates structural lattice defects, are the main responsible for the CNTs radical scavenging activity. Moreover, the CNTs ability to entrap radicals can be profitably used for some biomedical applications [6] and for the protection of polymeric matrices against their oxidative degradation [3,7,8].

To enhance the CNTs radical scavenging activities, an innovative approach through the immobilization of moieties carrying specific anti-oxidant functionalities, has been proposed in literature [9–13]. In particular, the immobilization of the anti-oxidant moieties onto the CNTs surface can be carried out through chemical covalent linkage or physical adsorption. However, the immobilization of the synthetic anti-oxidant moieties, such as butylated hydroxytoluene (BHT) [9], hindered phenols [10] and hindered amine light stabilizers [11], through their chemical anchorage onto CNTs outer surface can be considered an useful method for enhancing the CNTs protection ability, gathering the active molecules at the polymer-nanofiller interface, which is critical area for the degradation of the polymer-based nanocomposites. Besides, the physical adsorption of the natural occurring moieties, such as vitamins [12] and polyphenols [13], onto CNTs surface is profitably fool

* Corresponding author.

https://doi.org/10.1016/j.ultsonch.2019.104807
Received 13 February 2019; Received in revised form 17 July 2019; Accepted 24 September 2019
Available online 25 September 2019

for enhancing the CNTs protection ability, also considering the action of the active molecules at the polymer-nanofiller interface, preserving the anti-oxidant integrity and functionalities.

According to the literature, the ultra-sound-assisted treatment is widely considered to improve the CNTs dispersion, breaking their aggregates due to the van der Waals forces [14], to assist the CNTs functionalization or to assist the formulation of nanocomposites [15,16]. However, as known, the cavitation phenomena during the ultrasound treatment causes the formation of structural defects on the CNTs surface, modifying their acceptor-like properties and aspect ratio [17].

Furthermore, the use of CB particles as UV stabilizer is well known and it is a consolidate practice for the rubber manufacturing industry. The CB particles ability to act as UV stabilizers for polymeric matrices can be understood considering their intrinsic capability to absorb UV-light. Unfortunately, the CB particles are inclined to form large particles aggregates into the polymeric matrices and their beneficial effect can be significantly compromised [18–20].

However, both CB and CNTs can form aggregates into the polymeric matrices and this can compromise their reinforcement and UV stabilization actions, because of the large aggregates can act as *"hotspots"*, accumulating energy and promoting the polymer oxidation [7,19].

However, currently, the G, CNTs and CB have been considered as suitable nanofillers for the formulation of advanced polymer-based nanocomposites because of the above mentioned peculiar properties of the carbonaceous nanoparticles. To obtain improved nanocomposites properties and performance in comparison to the neat polymer matrices, there is necessary to investigate accurately the preparation techniques and establish accurately the percolation behavior. As known, the achievement of good dispersion and distribution of the nanoparticles and the obtainment of formidable nanoparticles percolation network are hard matters and they require special attention and research solutions [21–25].

In this work, we propose an alternative approach to amplify and tune in a controlled way, the radical scavenging ability of CNTs and CB. Specifically, the CNTs and CB samples have been subjected to extended ultra-sound-assisted treatment for different time intervals (*i.e.* for 15′, 30′, 45′, 60′, 90′ and 120′). Therefore, due to the strong forces coming from the cavitation phenomena, the ultra-sound treatment of the carbonaceous nanoparticles causes two different simultaneous effects: (i) the disruption of the nanoparticles aggregates, and (ii) the capitalization of structural defects onto the nanoparticles surface, and at the same time, some carbon atoms from the outer surface change their hybridization from sp^2 to sp^3. Therefore, the ability of CNTs and CB, subjected to ultra-sound treatment for different time intervals, to entrap 1,1-diphenyl-2-pycryl (DPPH) radicals and to react with macro-radicals, coming from the photo-degradation of the UHMWPE matrix, has been accurately investigated and discussed.

2. Experimental part

2.1. Materials

Ultra High Molecular Weight Polyethylene, UHMWPE, is a commercial grade purchased by Sigma-Aldrich in the form of a white powder. Its main properties are: average molecular weight $M_w = 3 \div 6$ MDa, softening point $T = 136$ °C (ASTM D 1525B: Vicat Softening Temperature), melting point $T_m = 138$ °C, degree of crystallinity about 48.1% (estimated through DSC measurement considering a heat of fusion for perfectly crystalline polyethylene $\Delta H_f = 288.84$ J/g), and density $\rho = 0.94$ g/mL at 25 °C. The viscosimetric average molecular weight, estimated from three independent measures of the intrinsic viscosity, and, considering the Margolies equation (according to ASTM D4020-05: Standard Specification for Ultra-High-Molecular-Weight Polyethylene Molding and Extrusion Materials, using a Lauda Pro-line PV15 viscometer), is $Mv = 5.37*10^4\,[g/mol]^{1.37}$, was $Mv \cong 4.9*10^6$ g/mol.

Multiwalled Carbon Nanotubes, CNTs, were prepared by the typical Chemical Vapor Deposition (CVD) protocol, using ethylene as carbon source [1] and a catalyst based on Fe supported on alumina. The purification was performed with 50% aqueous sulfuric acid, obtaining carbon nanotubes with outer diameters ranging between 14 and 20 nm, inner diameters in the range of 2 to 5 nm, length $1 \div 10$ μm, and purity > 96 wt%. Moreover, after the purification process the content of carboxylic groups was estimated to be about 0.5% by means of XPS analysis and acid/base titration.

All chemicals and reagents were used as received, without further purification.

Carbon black, CB, (Super P®) is a fine black powder and it has been supplied by MTI Corporation, Richmond, CA 94804–3809, USA. Its main properties are: density: 0.16 g/cm^3; volatiles ≤ 0.15%; particles size = 40 nm; specific surface area = 62 m^2/g; ash ≤ 0.10%.

2.2. CNTs and CB sonication

All the sonication were performed using an ultrasonic cell disruptor Branson Sonifier 250 equipped with a 1/2″ Tapped Bio Horn 101-147-037. Samples of 2 g of CNTs and of CB were separately placed in a 500 mL beacker with 250 mL of distilled water and 50 mL of acetone. The resulting suspension were sonicated for the different time intervals, specifically, for 15′, 30′, 45′, 60′, 90′ and 120′, with the power set on 20 W and keeping the temperature below 30 °C by means of an ice bath; then the CNTs and CB suspensions in water/acetone were filtered and dried at 80 °C overnight.

2.3. Nanocomposite preparation

The UHMWPE (white powder) and 1 wt% of CNTs and CB (specifically, untreated nanoparticles (0′) and us treated nanoparticles for different time intervals, (*i.e.* for 15′, 30′, 45′, 60′, 90′ and 120′)) were manually mixed at room temperature and the resulting powder has been homogenized by thorough grinding in a porcelain mortar up to the formation of visually homogeneous grey powder blends. Afterwards, the resulted visually homogeneous blends (UHMWPE/CNTs and UHMWPE/CB composite blends, containing untreated nanoparticles and us treated nanoparticles), have been subjected to magnetic stirring for about 12 h, until the achievement of a totally homogeneous black powder blends. The color change, from grey to black, of the UHMWPE/CNTs and UHMWPE/CB powder blends has been taken into account as a visual indicator for good nanoparticles dispersion and distribution into the UHMWPE. Therefore, the stirring time for about 12 h has been chosen, because upon further stirring, the homogeneous black powder blends do not changed.

Then the obtained black powder blends were hot compacted at 210 °C for 5 min and under a pressure of 1500 psi to get thin films (thickness less than 100 μm) for the subsequent analyses.

The neat UHMWPE was subjected to the same procedure for comparison.

2.4. Characterization

Micro-Raman spectroscopy has been performed at room temperature through a Renishaw Invia Raman Microscope equipped with a 532 nm Nd:YAG laser excitation and 100 mW power. Non-confocal measurements were carried out in the range 3200–100 cm^{-1} with a spectral resolution between 0.5 and 1 cm^{-1}.

The 1,1-diphenyl-2-pycryl (DPPH, supplied by Sigma-Aldrich) free radical scavenging assay was carried out according to published procedures [26,27]. Samples for a typical measurement were prepared by placing in a screw-capped vial 2 mg of functionalized carbon nanotube, to which 2 mL of a methanol solution of DPPH (10^{-4} M) were added. All samples were thermostated at 25 °C for the time required by the

measurement. Then the supernatant liquid was removed and the UV–vis spectrum recorded in a Beckmann DU-800 spectrometer. Spectra were recorded on a spectrophotometer equipped with a Peltier temperature controller. Scavenging activities were determined from the drop in absorbance at 517 nm of each sample compared with that of the DPPH solution in the absence of contact with the material. Scavenging efficiency values were calculated by Eq. (1) [26].

$$\text{Radical Scavenging Efficiency (\%)} = \frac{A - B}{A - 0.10} \times 100 \quad (1)$$

were A is the absorbance of the DPPH solution and B that of the DPPH solution after contact with the materials.

Dynamic light scattering measurements on the high diluted CNTs or CB dispersions (10^{-3} w/w%) were carried out using a Zetasizer NANO-ZS (Malvern Instruments). A 5 mM sodium dodecyl sulphate (SDS) aqueous solution was used to improve the CNTs and CB colloidal stability. The field-time autocorrelation functions were analyzed by Inverse Laplace Transformation (ILT) that provide the distribution of the decay rates (Γ) for the diffusive modes. For the translational motion, the collective diffusion coefficient (D) given by $D = \Gamma/q^2$, where q is the scattering vector ($4\pi n\lambda - 1 \sin(\theta/2)$; with n being the water refractive index, λ the wavelength (632.8 nm), and θ the scattering angle (173°)). The distribution of the apparent hydrodynamic diameters (D_h) was calculated by using the Stokes-Einstein equation. It should be noted that the Dh values for non-spherical particles is related to the translational diffusion dynamic of the colloidal object representing the radius of the sphere with equivalent diffusion mobility. In principle, the actual value of the characteristic sizes of nanotubes is correlated to the apparent hydrodynamic by considering that [28]

$$D_h = \frac{2L}{2\ s - 0.19 - 8.24/s + 12/s^2} \quad (2)$$

being L the aggregate length and s = ln(L/r) with r being the radius of the nanoparticles aggregates.

Transmission Electron Microscopy (TEM) analyses were performed on a homogeneous dispersion of the CNTs and CB in 2% aqueous sodium dodecyl sulfate (SDS, supplied by Sigma-Aldrich) using a Philips CM 200 field emission gun microscope operating at an accelerating voltage of 200 kV. A Gatan US 1000 CCD camera was used and 2048x2048 pixels images with 256 grey levels were recorded. For the specimen preparation few drops of the water solutions were deposited on 200 mesh lacey carbon-coated copper grid and air-dried for several hours before analysis.

Thermo-Gravimetric Analysis (TGA) was performed on a PerkinElmer STA 6000 thermal analyser; the samples were heated from 35 °C to 900 °C (10 °C/min) in nitrogen atmosphere.

Crystallization behaviour of neat UHMWPE and formulated nanocomposites has been investigated by Differential scanning calorimetry (DSC), using a Perkin-Elmer DSC7 calorimeter. All experiments were performed under dry N_2 gas using samples of around 10 mg in 40 μL sealed aluminium pans. Four calorimetric scans (two heating: 30–180 °C and two cooling: 180–30 °C) were performed for each sample at scanning heating/cooling rate of 10 °C/min.

The crystallinity degree (X_c) is calculated using the formula:

$$X_c(\%) = \frac{\Delta H_m}{\Delta H^0(1 - W_f)} \quad (3)$$

where ΔH_m is the heat of melt of sample, ΔH° is the heat of fusion for 100% crystalline UHMWPE (289 J/g) and W_f the mass fraction of the nanofiller [10,11]. The reported results are the average of three independent measurements.

The photo-oxidative resistance of the samples was estimated using a Q-UV-Solar Eye weatherometer (from Q-LAB, USA) equipped with UVB lamps (313 nm), at T = 55 °C.

The progress of the photo-oxidative degradation was followed by analysing the evolution in time of FTIR spectra on polymer films carried out by using a Perkin Elmer FT-IR spectrometer (mod. Spectrum Two). FTIR spectra collected on three different films of each sample were obtained by performing 16 scans between 4000 and 500 cm^{-1}. The photo-oxidation evolution was quantified by referring to the carbonyl index (CI) as a function of degradation time. CI was calculated as the ratio between the integral of the carbonyl absorption region (1850–1600 cm^{-1}) and that of a reference peak at about 2019 cm^{-1}, which accounts for the sample thickness variation and remains almost unchanged upon UVB exposure. The carbonyl absorption peak reflects the overall accumulation of all the oxygen containing groups, which are formed upon the UVB exposure.

3. Results and discussion

3.1. Radical scavenging activity of usCNTs and usCB

To assess the effectiveness of ultra-sound treatment on CNTs and CB abilities in trapping DPPH radicals, methanol mixtures of usCNTs/DPPH and usCB/DPPH have been prepared and analyzed via UV–vis spectrometry. As above mentioned, to amplify and tune in a controlled way, the radical scavenging activity of the carbonaceous nanoparticle, the usCNTs and usCB have been subjected to us treatment for different time intervals, *i.e.* 0′, 15′, 30′, 45, 60′, 90′ and 120′. Furthermore, the radical scavenging efficiencies of usCNTs and usCB to entrap DPPH radicals after 24 h, 120 h and 240 h (specifically, short, medium and extended contact/reaction time for both usCNTs/DPPH and usCB/DPPH systems) have been calculated using eq. (1) and in Fig. 1(a and b), the trends of calculated values as a function of the ultrasound time are plotted, respectively. It can be observed than the radical scavenging efficiencies for usCNTs and usCB are higher than that for untreated CNTs and CB for all considered time intervals, *i.e.* 24 h, 120 h and 240 h, and they increase progressively as a function of the us treatment time. It is worth noting two particular issues: (i) usCB show higher trapping abilities than usCNTs, especially at prolonged contact times, (ii) usCB is able to entrap more DPPH radicals for 120 h contact time rather than for 240 h.

Besides, all UV–vis spectra, collected after 24 h, 120 h and 240 h, of the methanol suspensions of usCNTs/DPPH and usCB/DPPH (usCNTs and usCB subjected to us treatment for different time intervals), are reported as supplementary figures, see Fig. S1. The typical DPPH absorption band at 517 nm is clearly visible in the spectra of DPPH/MeOH and the intensity of this bands significantly decreases in the presence of both kinds of carbonaceous nanoparticles, because of their ability to entrap DPPH radicals. The intensity decrease of band at 517 nm is more pronounced for both kinds of sonicated carbonaceous nanoparticles and it appears more marked at extended ultrasound time intervals.

To assess the effect of ultrasound treatment on the formation of structural defects and on the variation of the overall nanoparticles dimensions, Raman analysis and dynamic light scattering measurements (DLS) of usCNTs and usCB treated for different time intervals have been carried out, also according literature [30,31]. As known, the Raman spectra of the carbonaceous nanoparticles show two well different peaks, specifically, centered at 1340 cm^{-1} and 1580 cm^{-1} and named defect induced disorder mode (D-band) and tangential mode (G-band), respectively. Furthermore, the ratio between the intensities of these two specific Raman bands, *i.e.* I_D/I_G, can be considered as a valuable tool to qualitatively evaluate the defects concentrations, before and after the us treatment, of both kinds carbonaceous nanoparticles. In Fig. 2(a and b), the I_D/I_G ratio trends of usCNTs and usCB treated for different time intervals are plotted, respectively, and it can be noticed that I_D/I_G ratio increase for both kinds carbonaceous nanoparticles, and this increase is more pronounced for usCNTs. The I_D/I_G ratio for the untreated CNTs is about 0.96 and it becomes 1.17 for usCNTs treated for 120 min and this could be understood considering that the prolonged us treatment leads to damage of the CNTs graphitic structure and to formation of non-graphitic hybrid structure. Further, the I_D/I_G ratio for the untreated CB

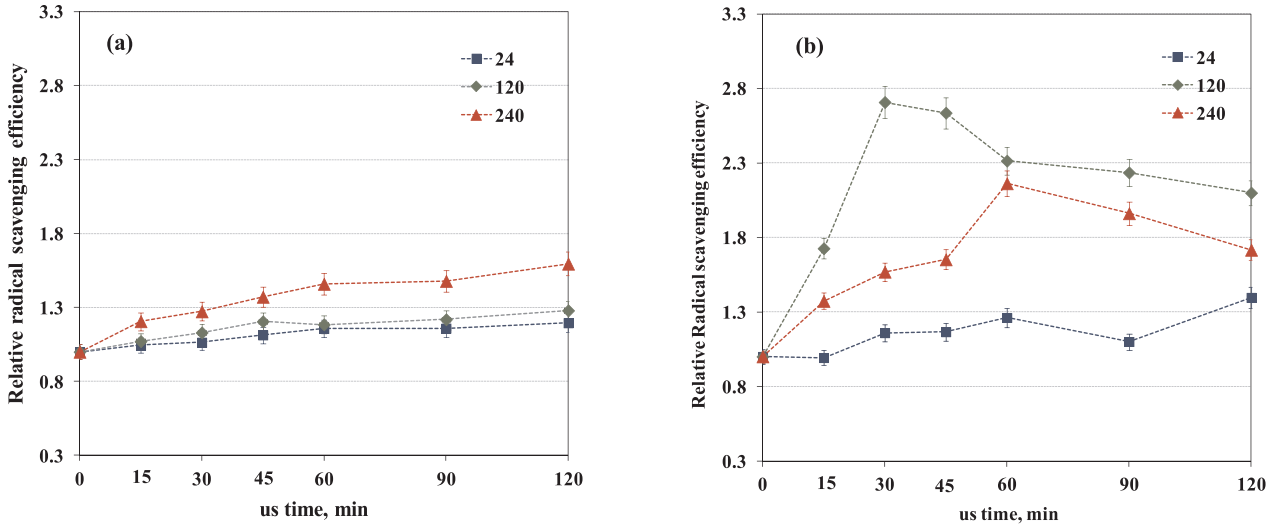

Fig. 1. Relative radical scavenging efficiency in trapping DPPH radicals after 24 h, 120 h and 240 h of (a) usCNTs and (b) usCB sonicated for different time intervals.

is about 0.98 and it becomes 1.06 for usCB treated for 120 min. Besides, all obtained Raman spectra are reported as Supplementary information in Fig. S2.

The formation of some structural defects on the carbonaceous nanoparticles, induced by the us treatment, can lead also to the variation of the overall nanoparticles dimensions. As known in literature, the average apparent hydrodynamic diameters are related to the characteristic lengths of the anisotropic nanoparticle aggregates, and besides, to the shell hydration and aggregation phenomena. Indeed, the apparent hydrodynamic diameter of the nanoparticles can be related to the translational diffusion behavior of the scattering objects and it can be correlated to the actual nanoparticles characteristic sizes [29]. The average hydrodynamic diameters for usCNTs and usCB, sonicated for different time intervals, have been calculated considering the translation diffusion coefficient from DLS experiments and Fig. 3(a and b) reports the trends of obtained average hydrodynamic diameter as a function of the sonication time are reported. The obtained distribution function of apparent hydrodynamic diameters for all investigated samples are reported as Supplementary information, see Fig. S3. It is worth noting that even if the average hydrodynamic diameters for usCNTs and usCB are not strictly comparable, because of CNTs and CB different shapes, *i.e.* CNTs cylindrical nanoparticles and CB spherical nanoparticles, and their length/diameter (l/d) ratio are different. Therefore, both trends in Fig. 3 clearly show that the us treatment leads to decrease of the overall dimensions of the nanoparticles aggregates. Overall, the reduction of the average hydrodynamic diameter for usCNTs-120, in comparison to the usCNTs, is more pronounced (about five times), than that the reduction observed for usCB-120, which is less than two times. The latter is also supported by TEM observations for both kinds considered carbonaceous nanoparticles, see insets in Fig. 3.

Additional TGA analysis on both CNTs and CB before and after extended us treatment at 120′ has been performed and in the TGA curves are reported as supplementary figures, see Fig. S5. As expected, no significant difference in the TGA trends before and after us treatment for both CNTs and CB nanoparticles has been detected and it can be supposed that the us treatment influences the overall nanoparticles structural arrangement, as demonstrated by Raman analysis and by the estimation of the apparent hydrodynamic diameter for both CNTs and CB nanoparticles, above discussed.

Let's discuss about a particular phenomenon observed for usCB, specifically, the usCB/distilled water suspensions show a clear tendency to separate in two different fractions, *i.e.* floating and precipitate

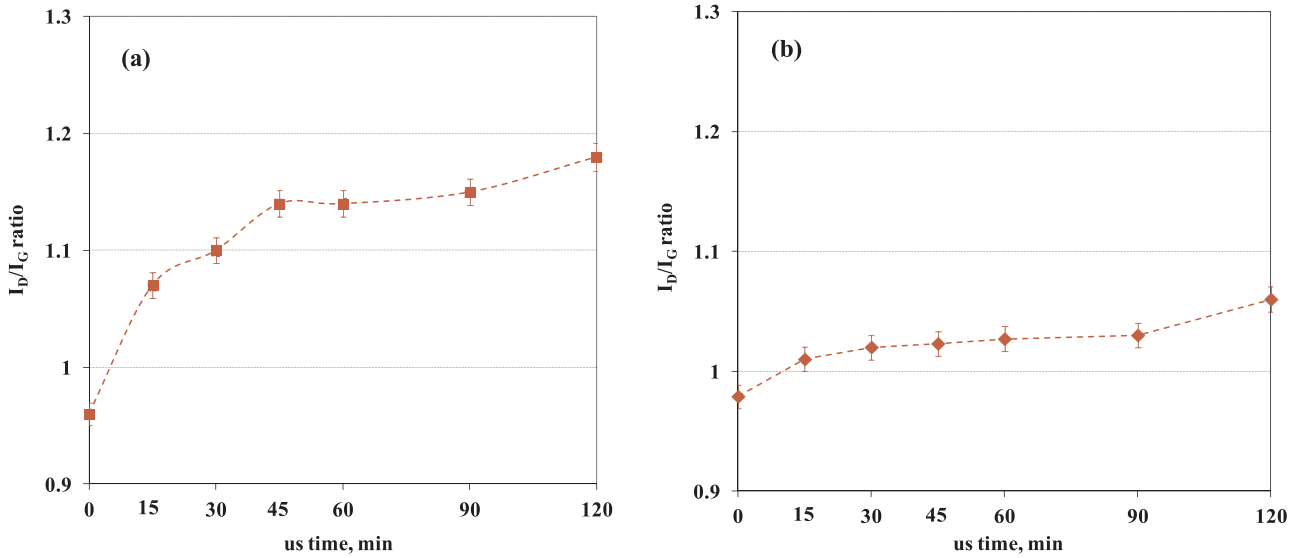

Fig. 2. I_D/I_G ratio of (a) usCNTs and (b) usCB sonicated for different time intervals.

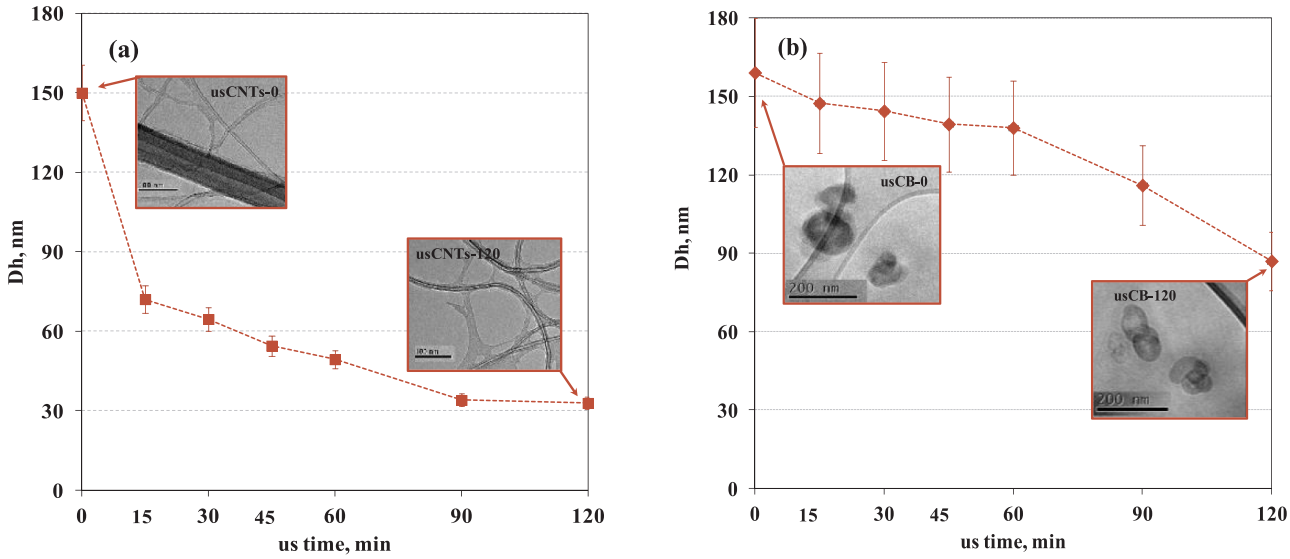

Fig. 3. Apparent hydrodynamic diameter, Dh, and TEM images of (a) usCNTs and (b) usCB sonicated for different time intervals.

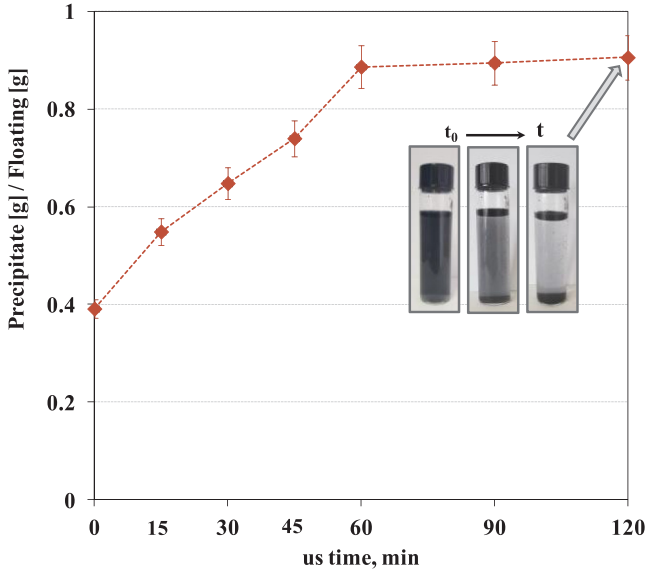

Fig. 4. Precipitate/Floating ratio of usCB fractions as a function of us time intervals.

fractions, and this tendency becomes more pronounced for usCB subjected to prolonged us time intervals. In Fig. 4, the weight ratio between the precipitate and floating fractions for usCB sonicated for different time intervals are shown and it is evident that the values of this ratio increase with increasing the us treatment time up to 60 min, after that this ratio remains almost unchanged up to 120 min of us treatment. Additionally, the inset pictures in Fig. 4 show the occurred separation phenomena for usCB-120, which takes place for time intervals at about 24 h. Indeed, immediately after the preparation of CB/distilled water suspension, the CB nanoparticles are likely to float, because of their very low apparent density, but at the same time, their motions cause the collisions, and subsequently, the formation of precipitate fraction is favored.

Therefore, the formation of precipitate fraction proceeds up to achievement of an apparent balance between the floating and precipitate fraction is noticed and the latter is clearly pronounced for the samples subjected at prolonged us time intervals, *i.e.* from 60′ to 120′. As discussed above, the us treatment of the CB nanoparticles leads to reduction of their apparent hydrodynamic diameter, but contemporary, begins the collisions between these smaller spherical particles, which leads to the formation of precipitate CB fractions. The collision phenomena for the CNTs nanoparticles is not observed, maybe because it is not favored, considering the CNTs specific shape and high value of length/diameter ratio.

Therefore, the formation of secondary CB aggregates, after the us treatment, that make up the CB precipitate fraction in the CB/water suspension, is noticed, and just the formation of these secondary CB aggregates could be invoked in order to explain the unexpected results related to higher ability of usCB to scavenge DPPH radicals for contact/reaction time at 120 h, rather than at 240 h. Probably, the formation of secondary aggregates in the methanol mixtures of usCB/DPPH after 240 h contact/reaction time, takes place and it is a predominant phenomenon, than the DPPH radicals scavenging. The formed precipitated CB aggregates have larger dimensions and their active surface decreases, and expectedly, the DPPH radicals scavenging efficiency decreases.

However, based on all obtained results, the us treatment can be profitably used: (i) to prevent the aggregation and agglomeration of the carbonaceous nanoparticles and (ii) to induce structural defects in both kinds carbonaceous nanoparticles by tuning the us time intervals. A possible action mechanism of us treatment on CNTs and CB is schematically represented in Fig. 5.

Therefore, it can be supposed that the us treatment is able to destroy the CNTs aggregates and bundles, see scheme (A), and it is significantly effective for short time intervals, *i.e.* up to 15 min. This supposition reflects the decreasing trend, even more pronounced up to 15 min of us treatment, of the apparent hydrodynamic diameter for CNTs. Concerning the CB nanoparticles, the us treatment is able to reduces the formation of agglomerates and aggregates, leading to the formation of small aggregates, consisting a few nanoparticles, and single nanoparticles, see scheme (B), in agreement with the decreasing Dh trend.

Further, the us treatment can be profitably used to induce some structural defects on the carbonaceous nanoparticles by tuning the us time intervals, as also confirmed by Raman analysis. Mostly, the modification of acceptor-like properties of the carbonaceous nanoparticles leads to change of the hybridization from sp^2 to sp3 of some carbonaceous atoms from the outer surface, as also theoretically predicted by DFT [3,4], inducing in this way radical scavenging ability.

However, further confirmation that the increased content of the structural defects, due to the us treatment, can be considered responsible for improved radical scavenging activity of both kinds carbonaceous nanoparticles, comes from the exemplification of the relative

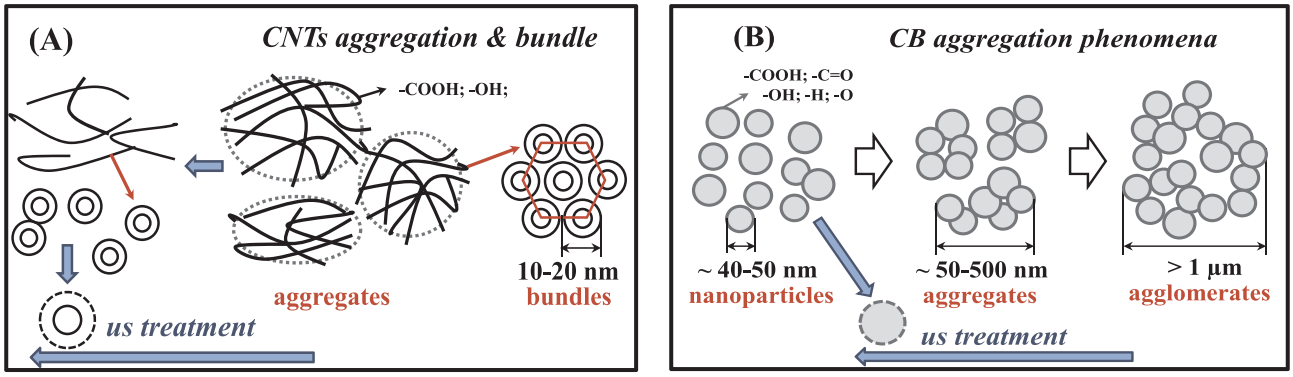

Fig. 5. Schematic representation of CNTs & CB aggregation phenomena and us treatment action.

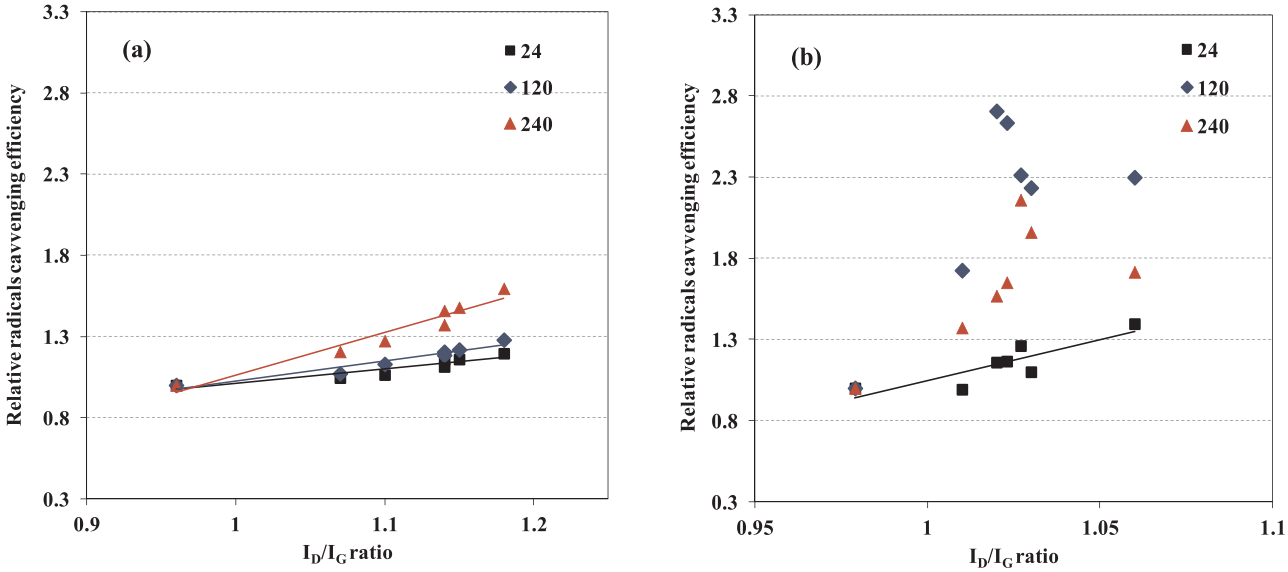

Fig. 6. Relative radical scavenging efficiency in trapping DPPH radicals vs I_D/I_G ratio for (a) usCNTs and (b) usCB.

radical scavenging efficiency as a function of the I_D/I_G ratio, see Fig. 6.

It can be observed that the radical scavenging efficiency of well-ordered CNTs toward DPPH radicals depends linearly on the I_D/I_G ratio for all considered contact times, *i.e.* 24 h, 120 h and 240 h, see Fig. 6(a), highlighting clearly that the enhanced ability to scavenge free radicals of usCNTs can be attributed to the achieved structural defects, due to the ultrasound treatment. The considerations for the disordered CB are much more complex, specifically: (i) the radical scavenging efficiency depends linearly on the I_D/I_G ratio only at lowest contact times, *i.e.* 24 h, between usCB and DPPH radicals, see Fig. 6(b); (ii) at longer contact times, *i.e.* 120 h and 240 h, the radical scavenging efficiency of usCB is affected by two contracting phenomena: first, ability to scavenge radicals, and second, the formation of CB secondary aggregates, and it results the balance between these two contrasting phenomena.

Finally, to sum up, controlling the us treatment time intervals, carbonaceous nanoparticles with tuned and tailored radical scavenging efficiency can be obtained, also considering that the content of the achieved structural defects, due to the us treatment, regulates and determinates their radical scavenging activity.

3.2. Photo-oxidation resistance of UHMWPE-based nanocomposites

First of all, a preliminary DSC analysis on the neat UHMWPE and UHMWPE-based nanocomposites containing CNTs and CB before and after prolonged us treatment for 120′ has been carried out and the obtained results are reported in Table 1 and Fig. S6. The presence of both kinds of carbonaceous nanoparticles leads to a slight decrease of the crystallinity degree, in comparison to the value obtained for neat UHMWPE, and this decrease is more pronounced for the nanocomposites containing us treated CNTs and CB nanoparticles. The latter could be understand considering that the prolonged us treatment leads to the disruption of the CNTs and CB aggregates, as well as the accumulation of structural defects, and the formation of nanoparticles with reduced dimensions is favored. Therefore, these smaller nanoparticles hinder the formation of crystalline structure in the host UHMWPE matrices and for this reason, the crystallinity degree decreases. Besides, the formation of secondary nanoparticles aggregates is not favored in the nanocomposites because of high intrinsic melt viscosity of neat UHMWPE during processing.

Overall, it is worth noting that the oxidation phenomena at room temperature for the polymer-based nanocomposites having larger

Table 1
Calorimetric data, *i.e.* fusion temperature (T_f), fusion enthalpy (ΔH_f) and calculated crystallinity degree, evaluated at the second heating scan, for neat UHMWPE and some UHMWPE-based nanocomposites.

Sample	T_f, °C	ΔH_f, J/g	Crystallinity Degree, %
UHMWPE	131.6	139.1	47.5
UHMWPE/CNTs	131.1	134.2	46.9
UHMWPE/usCNTs-120	130.7	122.3	43.0
UHMWPE/CB	131.1	136.5	47.2
UHMWPE/usCB-120	128.8	121.8	42.2

amorphous content, are usually favored, in comparison to oxidation phenomena which undergo samples having high crystallinity degree, because of easy oxygen penetration and diffusion into the amorphous phase [10–13].

The ability of usCNTs and usCB to improve the photo-oxidation resistance of UHMWPE-based nanocomposites has been evaluated subjecting thin films to UVB exposure. The progress of the degradation phenomena has been monitored through the analysis of the evolution time of the FTIR spectra. In particular, the photo- oxidation processes of neat UHMWPE and all UHMWPE-based nanocomposites, containing usCNTs and usCB sonicated at different time intervals, lead to the overall accumulation of carboxylic acids, ketones, esters and lactones, which formation reflects the growth of a complex peak in the range 1850–1600 cm^{-1}, aslo according to the literature [3,7,10–13,31]. Besides, the presence of carbonaceous nanoparticles does not affect the oxidation mechanisms of UHMWPE, leading to the formation of the same oxygen-containing species, some obtained spectra are reported as Supplementary information, see Fig. S4. The overall accumulations of oxygen-containing groups during the UVB exposure, named Carbonyl Index, have been calculated as a ratio between the area of peak in the range 1850–1600 cm^{-1} and the area of bending vibration area of the $–CH_3$ at 2019 cm^{-1}. Furthermore, in Fig. 7(a and b), the Carbonyl Index during the photo-oxidation of neat UHMWPE and all investigated nanocomposites UHMWPE/usCNTs and UHMWPE/usCB, containing nanoparticles sonicated at different time intervals, as a function of the exposure time are reported, respectively. The neat UHMWPE shows a rapid growth of the oxygen-containing groups during the UVB exposure, indicating that the degradation process begins in the early stage of the exposure, while, the all nanocomposites, containing usCNTs and usCB sonicated at different time intervals, demonstrate less pronounced accumulation of the oxygen-containing groups with respect to the neat matrix.

It is worth noting that the neat UHMWPE after about 168 h of UVB exposure becomes totally brittle and on this sample further analysis cannot be performed. All nanocomposites also after about 450 h of exposure are not brittle, although the values of carbonyl index increase. The anti-oxidant activity of untreated CNTs, and even more of usCNTs, is evident and their stabilizing action progressively increase with increasing the us time. Besides, the adding of CNTs and usCNTs leads to an increase of the induction time for the photo-oxidation degradation, *i.e.* conventionally calculated as the time at which the carbonyl index reaches values of 5, see inset reported in Fig. 7(a); it indicates an increase of the beginning time of the oxidation process. Exactly, the same considerations can be made for CB, untreated CB and usCB nanoparticles are able to prevent the UHMWPE photo-oxidation, as clearly noticeable in Fig. 7(b). Really, the usCB nanoparticles protect the UHMWPE more efficiently in comparison to the usCNTs because of the their well-known intrinsic ability to adsorb UV irradiation, reason why these nanoparticles are used at large industrial level as UV stabilizers and rubber reinforcement particles.

Interestingly, it is worth notice that the UHMWPE-based nanocomposites containing usCNTs-120 and usCB-120 show highest photo-oxidation resistance, although their crystallinity degree is lower than that to neat UHMWPE and UHMWPE-based nanocomposites containing untreated CNTs and CB. The latter could be understand considering that the us treatment has significantly improved the radical scavenging ability of both CNTs and CB towards polymer macro-radicals coming from the degradation of the UHMWPE matrix, though the lower crystallinity degree favors the oxygen penetration.

Anyway, both kinds carbonaceous nanoparticles are able to exert radical scavenging activity also towards polymer macro-radicals, due to their intrinsic properties, and this ability is significantly exacerbated by the us treatment. However, the us treatment of both usCNTs and usCB leads to destruction of the aggregations and to capitalization of structural defects, and the amount of these defects increase with increasing the us treatment time. In fact, the CNTs and CB, and even more usCNTs and usCN, are able to entrap the polymer macro-radicals coming from the photo-oxidation process of the polymeric matrix.

4. Conclusions

In this work, the radical scavenging ability of usCNTs and usCB, sonicated at different time intervals, toward DPPH radicals and polymer macro-radicals has been investigated and compared to that exerted by untreated CNTs and CB. The us treatment of CNTs and CB leads to disruption of the nanoparticles aggregations and to capitalization of structural defects, which amount increases with increasing the us treatment time. As demonstrated, the increased content of CNTs and CB defects, achieved during the us sonication time, leads to an increased reactivity toward 1,1-diphenyl-2-pycryl (DPPH) and an enhanced anti-oxidant activity toward macro-radicals, coming from the photo-degradation of the host polymer matrix.

Therefore, nanocomposites based on UHMWPE, containing untreated CNTs and CB and containing usCNTs and usCB sonicated at

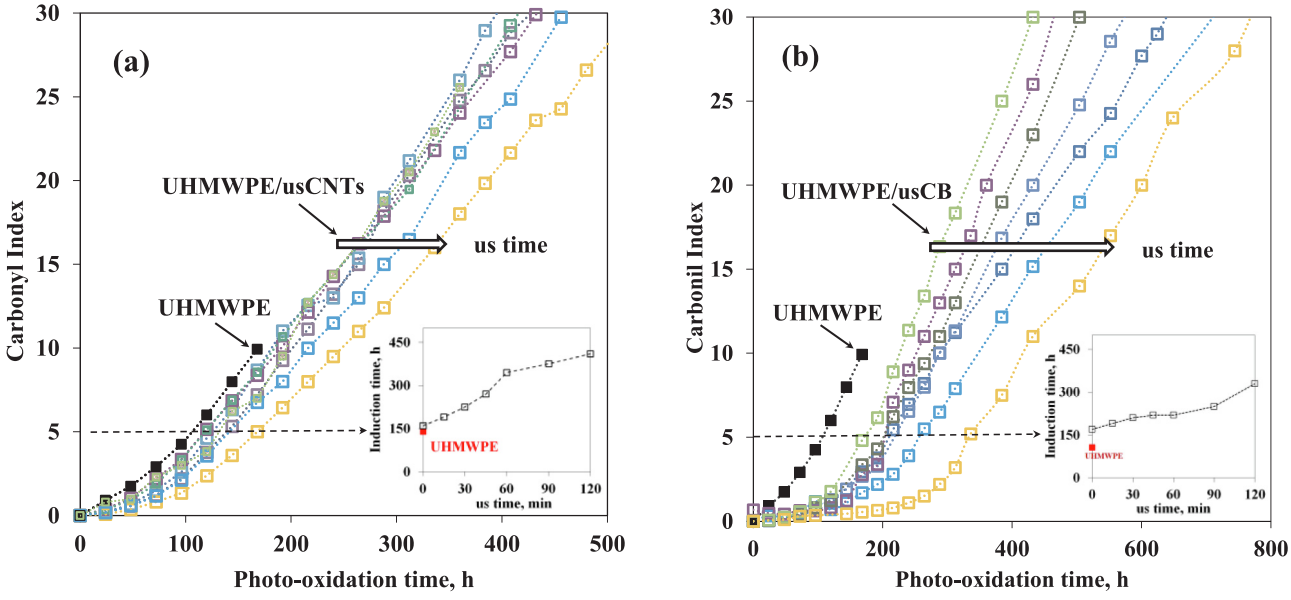

Fig. 7. Carbonyl Index of (a) UHMWPE/usCNTs and (b) UHMWPE/usCB containing usCNTs and usCB sonicated for different time intervals.

different time intervals, have been produced and their photo-oxidation resistance have been investigated. The photo-oxidation resistance of UHMWPE/usCNTs and UHMWPE/usCB is significantly improved in comparison to that of UHMWPE-based nanocomposites containing untreated CNTs and CB and of neat matrix.

Further, the capitalization of structural defects of both kinds carbonaceous nanoparticles, in a controlled way through the us treatment, can be considered responsible for their enhanced protection ability. The presence of large number of structural defects onto the carbonaceous outer surface leads to change of the hybridization of some carbon atoms from sp^2 to sp^3, enhancing in this way the radical scavenging activity toward DPPH radicals and polymer macro-radicals.

Appendix A. Supplementary data

Supplementary data to this article can be found online at https://doi.org/10.1016/j.ultsonch.2019.104807.

References

[1] P.J.F. Harris, Carbon Nanotube Science Synthesis, Properties and Applications, Cambridge University Press, UK, 2009.
[2] J.N. Coleman, U. Khan, W.J. Blau, Y.K. Gunko, Small but strong: a review of the mechanical properties of carbon nanotube-polymer composites, Carbon 44 (2006) 1624–1652.
[3] P.C.P. Watts, P.K. Fearon, W.K. Hsu, N.C. Billingham, H.W. Kroto, D.R.M. Walton, Carbon nanotubes as polymer antioxidant, J. Mater. Chem. 13 (3) (2003) 491–495.
[4] A. Galano, Carbon nanotubes as free-radical scavengers, J. Phys. Chem. C 112 (2008) 8922–8927.
[5] A. Martinez, A. Galano, Free radical scavenging activity of ultrashort single-walled carbon nanotubes with different structures through electron transfer reactions, J. Phys. Chem. C 144 (2010) 8184–8191.
[6] X. Li, Y. Fan, F. Watari, Current investigations into carbon nanotubes for biomedical application, Biomed. Mater. 5 (2010) 022001.
[7] N. Tz, F.P.La. Dintcheva, V. Malatesta Mantia, Photo-oxidation behaviour of polyethylene/multi-wall carbon nanotube composite films, Polym. Degrad. Stabil. 94 (2009) 162–170.
[8] I. Fenoglio, M. Tomatis, D. Lison, J. Muller, A. Fonseca, J.B. Nagy, et al., Reactivity of carbon nanotubes: Free radical generation or scavenging activity? Free Radical. Biol. Med. 40 (2006) 1227–1233.
[9] R.M. Lucente-Schultz, V.C. Moore, A.D. Leonard, B.K. Price, D.V. Kosynkin, M. Lu, et al., Antioxidant single-walled carbon nanotubes, J. Am. Chem. Soc. 131 (2009) 3934–3941.
[10] N.Tz. Dintcheva, R. Arrigo, C. Gambarotti, S. Carroccio, S. Coiai, G. Filippone, Advanced ultra-high molecular weight polyethylene/antioxidant-functionalized carbon nanotubes nanocomposites with improved thermo-oxidative resistance, J. Appl. Polym. Sci. 132 (2015) 42420–42428.
[11] N.Tz. Dintcheva, R. Arrigo, E. Morici, C. Gambarotti, S. Carroccio, F. Cicogna, et al., Multi-functional hindered amine light stabilizers-functionalized carbon nanotubes for advanced ultra-high molecular weight Polyethylene-based nanocomposites, Compos. Part B Eng. 82 (2015) 196–204.
[12] N.Tz. Dintcheva, R. Arrigo, C. Gambarotti, S. Carroccio, G. Filippone, F. Cicogna, et al., α-Tocopherol-induced radical scavenging activity in carbon nanotubes for thermo-oxidation resistant ultra-high molecular weight polyethylene-based nanocomposites, Carbon 74 (2014) 14–21.
[13] R. Arrigo, N.Tz. Dintcheva, M. Guenzi, C. Gambarotti, G. Filippone, S. Coiai, et al., Thermo-oxidative resistant nanocomposites containing novel hybrid-nanoparticles based on natural polyphenol and carbon nanotubes, Polym. Degrad. Stabil. 115 (2015) 129–137.
[14] S.M. Sabet, H. Mahfuz, J. Hashemi, M. Nezakat, J.A. Szpunar, Effects of sonication energy on the dispersion of carbon nanotubes in a vinyl ester matrix and associated thermo-mechanical properties, J. Mater. Sci. 50 (2015) 4729–4740.
[15] C. Park, Z. Ounaies, K.A. Watson, R.E. Crooks, J. Smith, S.E. Lowther, et al., Dispersion of single wall carbon nanotubes by in situ polymerization under sonication, Chem. Phys. Lett. 364 (2002) 303–308.
[16] X. Jia, F. Wei, Advances in production and applications of carbon nanotubes, Top Curr. Chem. 375 (2017) 18–53.
[17] F. Hennrich, R. Krupke, K. Arnold, J.A.R. Stutz, S. Lebedkin, T. Koch, et al., The mechanism of cavitation-induced scission of single-walled carbon nanotubes, J. Phys. Chem. B 111 (2007) 1932–1937.
[18] J.B. Donnet, R.C. Bansal, M.-J. Wang, Carbon Black: Science and Technology, 2nd Revised and Expanded Edition, CRC Taylor & Francis, New York, USA, 1993.
[19] K. Yurekli, R. Krishnamoorti, M.F. Tse, K.O. Mcelrath, A.H. Tsou, H.-C. Wang, Structure and dynamics of carbon black-filled elastomers, J. Polym. Sci.: Part B: Polym. Phys. 39 (2001) 256–275.
[20] J.-Ch. Huang, Carbon black filled conducting polymers and polymer blends, Adv. Polym. Technol. 21 (2002) 299–313.
[21] M.O. Lisunova, Y.P. Mamunya, N.I. Lebovka, A.V. Melezhyk, Percolation behaviour of ultrahigh molecular weight polyethylene/multi-walled carbon nanotubes composites, Europ. Polym. J. 43 (2007) 949–958.
[22] A. Mierczynska, M. Mayne-L'Hermite, G. Boiteux, J.K. Jeszka, Electrical and mechanical properties of carbon nanotube/ultrahigh-molecular-weight polyethylene composites prepared by a filler prelocalization method, J. Appl. Polym. Sci. 105 (2007) 158–168.
[23] C. Sanchez, B. Julián, P. Belleville, M. Popall, Applications of hybrid organic–inorganic nanocomposites, J. Mater. Chem. 15 (2005) 3559–3592.
[24] A.Y.W. Sham, S.M. Notley, A review of fundamental properties and applications of polymer–graphene hybrid materials, Soft Matter 9 (2013) 6645–6653.
[25] M.S. Saveleva, K. Eftekhari, A. Abalymov, T.E.L. Douglas, D. Volodkin, B.V. Parakhonskiy, A.G. Skirtach, Hierarchy of hybrid materials – the place of inorganics-in-organics in it, their composition and applications, Front. Chem. 7 (2019) 179.
[26] Y.T. Shieh, W.W. Wang, Radical scavenging efficiencies of modified and microwave-treated multiwalled carbon nanotubes, Carbon 79 (2014) 354–362.
[27] X. Zhang, M. Liu, X. Zhang, F. Deng, C. Zhou, J. Hui, et al., Interaction of tannic acid with carbon nanotubes: enhancement of dispersibility and biocompatibility, Toxycol. Res. 4 (2015) 160–168.
[28] K. Matsuoka, A. Yonekawa, M. Ishii, C. Honda, K. Endo, Y. Moroi, Y. Abe, T. Tamura, Micellar size, shape and counterion binding of N-(1,1-Dihydroperfluoroalkyl)-N, N, N-trimethylammonium chloride in aqueous solutions, Colloid Polym. Sci. 285 (2006) 323–330.
[29] L. Bokobza, J. Zhang, Raman spectroscopic characterization of multiwall carbon nanotubes and of composites, eXPRESS Polym. Lett. 6 (2012) 601–608.
[30] N.T. Dintcheva, R. Arrigo, R. Teresi, B. Megna, C. Gambarotti, S. Marullo, F. D'Anna, Tunable radical scavenging activity of carbon nanotubes through sonication, Carbon 107 (2016) 240–247.
[31] R. Arrigo, R. Teresi, C. Gambarotti, F. Parisi, G. Lazzara, N.Tz. Dintcheva, Sonication-induced modification of carbon nanotubes: effect on the rheological and thermo-oxidative behaviour of polymer-based nanocomposites, Materials 11 (2018) 383–396.